# Adhesion Mechanisms in the Solid-State Bonding Technique Using Submicrometer Aromatic Thermosetting Copolyester Adhesive

**Kun Xu,[1] John C. Selby,[2] Mark A. Shannon,[2] James Economy[1]**

[1]*Department of Materials Science and Engineering, University of Illinois at Urbana-Champaign, Urbana, Illinois 61801*
[2]*Department of Mechanical and Industrial Engineering, University of Illinois at Urbana-Champaign, Urbana, Illinois 61801*

Received 15 October 2003; accepted 19 December 2003

**ABSTRACT:** The adhesion mechanism between polyimides and aromatic thermosetting copolyester (ATSP) involved in the solid-state bonding technique using submicrometer ATSP coatings was evaluated. The adhesion strength at the interface between ATSP and polyimide is strongly related to the diffusion of ATSP into the polyimide base layer. We used dynamic secondary ion mass spectrometry to study the interface width between deuterated ATSP and polyimides and found that the interface between ATSP and poly(4,4′-diphenylether pyromellitimide) (PMDA-ODA) is wider than the interface between ATSP and poly(*p*-phenylene biphenyltetracarboximide) (BPDA-PPD) because of the less rigid chain in the PMDA-ODA. By partially curing both polyimides, the interface width was greatly increased, which could lead to an improved adhesion at the interface between polyimide BPDA-PPD and ATSP. © 2004 Wiley Periodicals, Inc. J Appl Polym Sci 92: 3843–3856, 2004

**Key words:** thin films; solid state bonding; aromatic thermoset; adhesion; polyimide

## INTRODUCTION

In microelectronic applications, good interfacial adhesion is essential to produce a reliable device. However, in such devices, poor adhesion often arises as a cause of failure between different materials or even between the same materials. One typical example is the adhesion problems of polyimide.

It is well known that polyimides have poor self-adhesion and poor adhesion to other substrates because of their anisotropy and semicrystalline structure.[1] Because polyimides are the most extensively used polymer in microelectronic industries, numerous studies have been conducted to solve polyimides' adhesion problems. Approaches to improve polyimides' adhesion include adding flexible structure into the polyimide backbone,[2] wet chemistry treating the surface of polyimide to reform polyamic acid,[3] partial curing[4] or solvent swelling the polyimide,[5] plasma activating the surface,[6] using Cr as adhesion promoter,[7] and applying adhesive,[8] etc. Most approaches were developed to solve specific interface problems involved with the sequential processing of polyimides. In such cases, enhancing the substrate's adhesion before coating polyimides or improving the adhesion of a cured polyimide base layer before depositing a top layer of a metal or another layer of polyimide fall in this category. It appeared to us that designing an adhesive that would address these problems would be highly desirable for the integration step at the end of a parallel process involved with polyimide. In a parallel process, individual components would be made and inspected and then integrated to make an assembled unit. For example, in microelectronic packaging, an adhesive could be used in the lamination of layers of lamina (where each layer contains polyimide dielectric and Cu circuits) into a multichip modules laminate (MCM-L). As another example, in the fabrication of microelectromechanical system (MEMS) devices, adhesive could be used to assemble and bond prefabricated MEMS components into an integrated device.[9] Because polyimides are extensively used in microelectronics and are involved in many of the integration processes, the desirable adhesive should have good adhesion with polyimides and with various other substrates. Other requirements for such adhesives include good thermal stability to sustain high-temperature processes that are often used in microelectronic fabrication and capability of being processed at submicrometer thicknesses to be compatible with the small features of microelectronic devices.

*Correspondence to:* K. Xu. 42628 Shoreham Park Court, Fremont, CA 94538 (kunxu2002@yahoo.com).

Contract grant sponsor: DARPA DSO; contract grant number: DABT63-97-C-0069.

Journal of Applied Polymer Science, Vol. 92, 3843–3856 (2004)
© 2004 Wiley Periodicals, Inc.

### Conventional adhesives

Currently, conventional polymer adhesives that are commonly used are acrylic, phenolic butyral, and epoxy-based systems. None of them have a thermal stability compatible with the high-temperature processes required for fabrication of polyimide. In cases where there are no requirements for high-temperature processing, it seems that acrylic or phenolic butyral could be used. However, both are easily attacked by moisture and solvents, so that the adhesion reliability could be a big concern. Among the three conventional adhesives, epoxy has the best thermal and chemical resistance but it is unstable at temperatures much above 180°C. Moreover, it tends to give a stiff composite structure and is difficult to process into very small bond line thicknesses.[8] Special microchannels have to be used to apply epoxy to the interface, which greatly complicates both the design and the fabrication.[10]

### High-temperature adhesives

Some high-temperature adhesives have been developed to solve the specific problems of interface adhesion related to polyimides. One example is a thermoplastic polyimide developed by DuPont, namely poly(4,4′-oxydiphenylene oxydiphthalimide) (ODPA-ODA) with a glass transition temperature of 270°C. It has been shown that this adhesive can improve the adhesion between polyimides.[8] However, due to the thermoplastic nature of ODPA-ODA, the bonding interface could lose its dimensional stability during high-temperature bonding, resulting in the movement of metal line (swimming). Another example is poly(arylene ether benzimidazole) (PAEBI), which has been studied as a polymeric primer to adhere copper and polyimide. PAEBI has good adhesion with copper because of the formation of PAEBI–copper complexes. However, its adhesion with polyimide needs to be enhanced by using wet chemistry treatment and plasma treatment of the polyimide.[11] In both approaches, hydrolytical instability might exist at the adhesive/substrate interface because both polymers have high moisture pickup.

### Use of ATSP

From previous studies, aromatic thermosetting copolyesters (ATSP) were found to display the following features: (1) two cured ATSP coatings could be bonded in the solid state via interchain transesterification reaction (ITR), greatly reducing the potential for void formation and guaranteeing the dimension stability at the bonding interface; (2) ATSP displayed excellent adhesion to metals such as Al, Ti, and steel, with 100% adhesion strength retention up to 150°C[12]; and (3) good adhesion was observed accidentally between polyimide and ATSP, when Kapton H® film was used as a release film in making ATSP composites. It was found to adhere surprisingly well to ATSP, and trying to separate them led to cohesive failure in Kapton H®.

Based on those unique properties of ATSP, the application of using ATSP as submicrometer thin film adhesive in microfabrication was exploited, as follows: (1) processes of solid-state bonding by using submicrometer thin-film ATSP were developed to enable the use of ATSP in the microfabrication world[13]; (2) adhesion strength with submicrometer bond line thicknesses were characterized and it was found ATSP had good adhesion with $SiO_2$, Cr, and polyimide[13]; and (3) submicrometer ATSP solid-state bonding technique was applied to a polyimide poly(4,4′-diphenylether pyromellitimide) (PMDA-ODA) membrane transfer process,[14] which, in turn, was used to assemble microfabricated components in a mesoscopic device—integrated mesoscopic cooling circuits (IMCC).[15]

While the application of ATSP as a submicrometer film adhesive in microelectronic devices has already been proved, it is the purpose of this article to develop an understanding of the adhesion mechanisms and, in particular, the mechanism between ATSP and polyimide. By synthesizing deuterated ATSP, dynamic secondary ion mass spectrometry (DSIMS) could be used to study the interface width between ATSP and polyimides.

## EXPERIMENTAL

### Materials

Trimesic acid (TMA) and isophthalic acid (IPA) were kindly provided by Amoco; hydroquinone (HQ), *p*-hydroxybenzoic acid (HBA), *p*-acetoxy benzoic acid (ABA), acetic anhydride, anhydrous *N*-methyl pyrrolidinone (NMP), concentrated sulfuric acid, and hydrochloric acid were purchased from Aldrich. Deuterium oxide, DMSO-$d_6$, and acetone-$d_6$ were purchased from Cambridge Isotopes. All chemicals were used as received.

Pyralin® polyimides PI-2611 [PI poly(*p*-phenylene biphenyltetracarboximide) (BPDA-PPD), solid % 13.1], PI-2613 (diluted PI-2611, solid % 5.8), and PI-2808 (PI PMDA-ODA, solid % 16.3) were purchased from HD MicroSystems and were used as received. PI-2808 was diluted from 16.3 to 5.8 wt % by using NMP. PI-2613 and diluted PI-2808 were used to prepare thin film samples for interface analyses. PI-2611 was used for bonding experiments. All polyimides were stored in a sealed container at −20°C and were taken out 12 h prior to use to prevent condensation. Four-inch silicon wafers (P-100-B type, 0.005–0.020 Ω/cm) were purchased from South West Silicon.

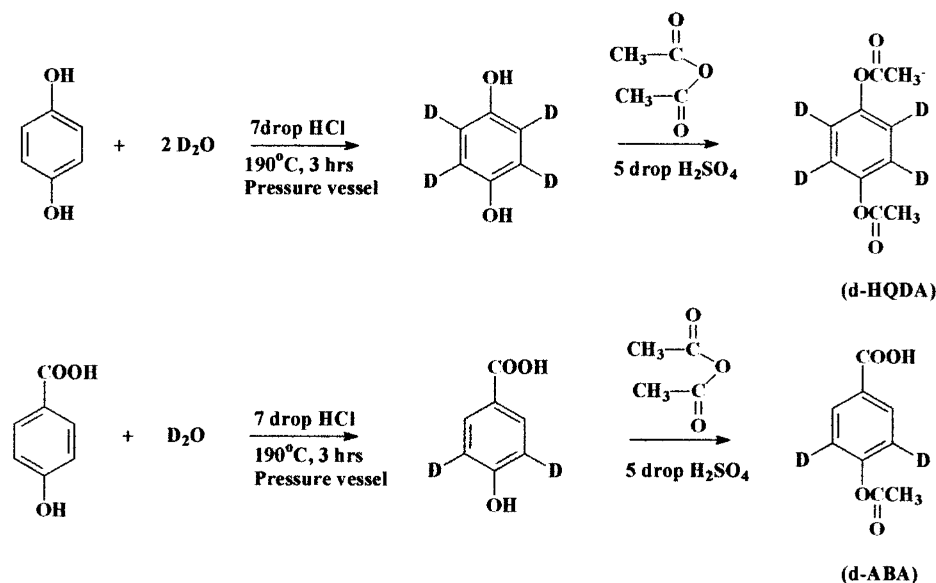


**Figure 1** Synthesis of deuterated HQDA (*d*-HQDA) and deuterated ABA (*d*-ABA).

### Equipment

All glassware were cleaned thoroughly in a KOH/NaOH base bath and dried in a 150°C oven prior to use. The stainless steel 47-mm pressure-filtration device (100 mL) and the type AW prefilter were purchased from Millipore Inc. The stainless steel pressure vessel was custom designed and machined in the Chemical Science School machine shop at the University of Illinois campus.

Thermal analyses of monomers and polymers were done by using either a TA Instruments modulated DSC 2910 or a TGA 2950 ramped at 10°C/min in a nitrogen atmosphere. $^1$H-NMR measurements were carried out by using a Varian Unity 400 NB NMR system with DMSO-$d_6$ and acetone-$d_6$ as solvents. The $^1$H-NMR data were analyzed by using NUTS software. The molecular weight and distribution were measured by using gel permeation chromatography (GPC). The characterization was performed by using NMP + 0.5*M* LiBr solvent in a 3× Plgel 10 $\mu$M Mixed B LS column at 25°C with a Waters 515 pump. Three detectors were used including a Viscotek HR 40 refractive index detector, a Viscotek T60A dual light scattering, and a differential pressure viscometer. A custom-built vacuum hot press was used in the bonding process of samples. Because the samples are small, a static weight was used to apply pressure instead of the hydraulic press. Five-pound brass weights were used to apply direct pressure on the 1 × 1 cm sample and the heating platens of the vacuum hot press were used to heat the samples during the bonding process.

A Hitachi S-4700 scanning electron microscope was used to observe the cross section of substrates bonded by ATSP by using 10-kV gun voltage. The sample was soaked in liquid $N_2$ and then fractured to expose the cross section. It was then sputtered with a 10-Å-thick platinum/gold layer before loading into the SEM chamber.

Digital Instruments MultiMode AFM was used to observe the surface topography of polyimide thin film in tapping mode. Nanodevices Metrology probe TAP 300 with resonant frequency of 300 kHz and spring constant of 40 N/m was used as the probe in the AFM studies. Nanoscope III 4.43r8 offline software was used to analyze AFM image.

DSIMS was performed on a Cameca IMS-5f instrument. A $Cs^+$ primary ion beam (14.5 keV, 35 nA) was used to sputter through the interface at ~ 3 Å/s sputtering rate, with a 250 × 250 $\mu$m raster area and a 10 × 10 $\mu$m detecting area. Similar to the sample preparation in SEM, samples were sputtered with a 10-Å Au layer to prevent static accumulation before loading into the SIMS chamber.

### Synthesis of deuterated hydroquinone (*d[b]-HQ)*

The synthetic path of deuterated monomers is illustrated in Figure 1. Synthesis of *d*-HQ was carried out in a 350-mL stainless steel pressure vessel equipped with magnetic stirring, thermocouple, pressure gauge, and vacuum/$N_2$ inlet. To this vessel, 30.36 g hydroquinone (274.6 mmol), 167.7 mL deuterium oxide (928.1 mmol), and seven drops of hydrochloride acid were added. After eliminating air by vacuum/$N_2$ purge three times, the pressure vessel was heated to 195°C in 1 h 25 min and kept at 195°C for 3 h while stirring. The pressure inside the vessel increased from 11 psi (room temperature, RT) to 180 psi (at 195°C)

and dropped to 11 psi after cooling to RT. When opening the pressure vessel, *d*-HQ was observed precipitated out from a green solution. The mixture was filtered and washed with deionized water. The crystalline flakes were collected and the filtered solution was extracted by using ether; ether was rotaevaporated to recover more *d*-HQ. The *d*-HQ was then dried at 70°C in a vacuum oven and 28.49 g *d*-HQ (91% yield) was obtained as final product.

### Synthesis of deuterated 4-hydroxy benzoic acid (*d[b]-HBA)*[16]

Synthesis of *d*-HBA was carried out in the same pressure vessel described in the previous reaction. To this vessel, 55.24 g HBA (400 mmol), 122.4 mL deuterium oxide (678 mmol), and 7 drops of hydrochloride acid were added and the reaction mixture was heated up to 195°C in 1 h 25 min and kept at 195°C for 3 h. The pressure inside the vessel increased from −9 psi (RT) to 554 psi (195°C). When cooling down to RT, about 200 psi pressure remained, indicating that some HBA had undergone decarboxylation resulting in phenol and carbon dioxide. After opening the vessel, the white solid was filtered and washed with DI water and dried at 75°C in a vacuum oven overnight to yield 26.85 g *d*-HBA (yield 48%).

### Synthesis of deuterated hydroquinone diacetate (*d[b]-HQDA)*

Synthesis of *d*-HQDA was carried out in a 300-mL three-necked flask equipped with $N_2$ inlet, condenser, mechanical stirrer, and thermometer. To this flask, 25 g *d*-HQ (232 mmol) and 100 mL acetic anhydride (1064 mmol) were added and heated to 100°C with mechanical stirring to dissolve HQ in acetic anhydride. The reaction mixture was cooled to 70°C and two drops of sulfuric acid was added into the reaction mixture, and the temperature was increased to 110°C due to the exothermic reaction. Crystals of HQDA were precipitated during the cooling. The reaction mixture was quenched in 50 mL DI water and the mixture was stirred for 1 h. The water-quenched mixture was then filtered and washed with 100 mL DI water until the pH was 5. The product was then dried at 50°C in a vacuum oven and 43.9 g HQDA was obtained as a final product with 93.6% yield.

### Synthesis of deuterated acetoxy benzoic acid (*d*-ABA)

Synthesis of *d*-ABA was carried out in a 300-mL three-necked flask equipped with mechanical stirrer, condenser, $N_2$ inlet, and thermometer. To this flask, a 25 g *d*-HBA (178.4 mmol) and 100 mL acetic anhydride (770 mmol) mixture was added. The reaction was heated to 85°C with stirring to allow *d*-HBA to dissolve in excess acetic anhydride. The temperature was lowered to 70°C and 5 drops of sulfuric acid were then added to the yellow–green solution. The reaction took place immediately and was completed in a few minutes. The reaction mixture was cooled down to RT and *d*-ABA solid was precipitated out. The mixture was poured into 1 L of DI water and stirred for 6 h. The mixture was then filtered and washed by using DI water, until the pH was 4. The final product was dried in a vacuum oven at 70°C to give 29.03 g *d*-ABA in 89% yield.

### Synthesis of deuterated A-1

In a 100-mL three-necked flask equipped with $N_2$ inlet, mechanical stirrer, thermometer, and refluxing condenser, 5.00 g TMA (23.8 mmol), 18.86 g *d*-HQDA (95.8 mmol), 3.95 g IPA (23.8 mmol), and 4.34 g *d*-ABA (23.8 mmol) were added. The chemical reaction to form A-1 was illustrated in Figure 2. Initially, the reaction was heated to 300°C in 30 min and acetic acid was allowed to reflux to wash sublimed HQDA back to the reaction mixture. The temperature inside the reactor was measured as around 210°C. After 2 h reflux, the reaction consisted of a mixture of solids and acetic acid. The reaction was cooled to RT and the refluxing condenser was replaced by a collecting condenser. Heating tape was wrapped around the distillation head and then the reaction was heated to 300°C to remove acetic acid (the inside temperature increased from 210 to 280°C with the removal of acetic acid). The reaction was stopped when 80% acetic acid was collected. The reaction mixture was clear orange melt. The stirring bar was raised above the melt and the reaction was allowed to cool to around 150°C; the melt was then poured out on a petri dish. The residual melt solidified easily and coated the flask inner wall. After the flask cooled to RT, liquid $N_2$ was poured into the reaction flask to debond the oligomer from glass by taking advantage of the coefficient of thermal expansion (CTE) mismatch between glass and the oligomer. The solid oligomer was broken into small pieces with the assistance of liquid $N_2$ and was then poured out from the reaction flask. The solid oligomer was then ground by using a coffee grinder.

### Synthesis of deuterated C-1

In the same 100-mL three-necked flask, 5.00 g TMA (23.8 mmol), 9.53 g *d*-HQDA (48.4 mmol), 5.93 g IPA (35.7 mmol), and 13.02 g *d*-ABA (71.4 mmol) were added. The reaction was carried out in a similar manner as in the small-scale synthesis of A-1. About 80% of the acetic acid was collected before the reaction was stopped.

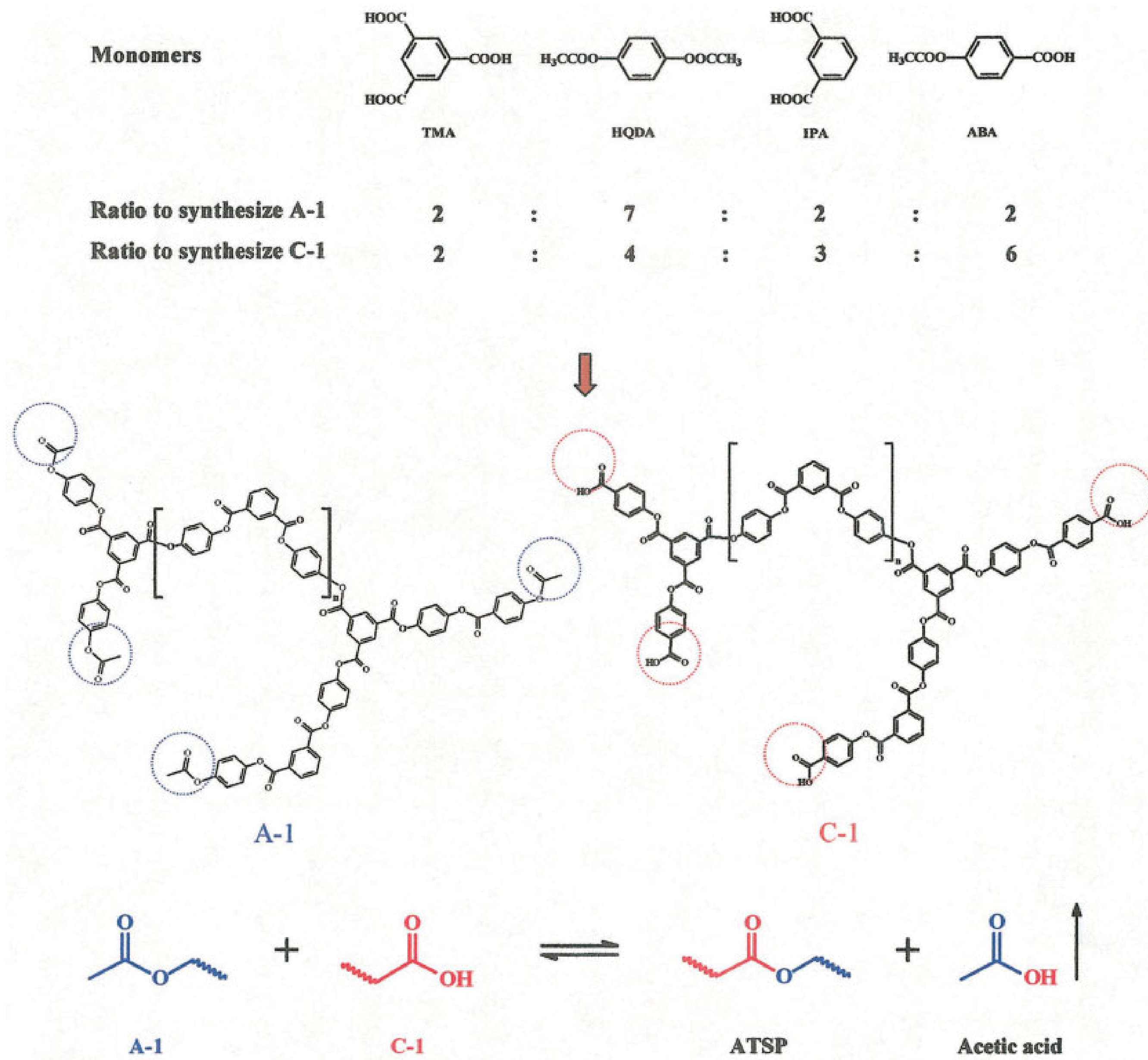


**Figure 2** Synthesis involved in ATSP system.

### Purification of ATSP oligomers for microfabrication

The oligomer was extracted by using DI water and methanol (1 : 3 by volume) for 24 h and dried at 70°C in a vacuum oven overnight. The purified oligomer was refined further by dissolving in NMP to make a 10% solution (by weight) and then filtered through a 1-$\mu$m glass fiber prefilter by using the Millipore pressure filtration device at 20 psi pressure. The filtered solution was precipitated in 10× volume of methanol and magnetically stirred for 4 h before vacuum filtration. The filtered white powder was extracted overnight by using methanol and dried at 70°C in a vacuum oven overnight. The yields of both A-1 and C-1 were about 55%. The ATSP oligomers, C-1 and A-1, were dissolved in NMP in a 1.1 : 1 weight ratio to make a 10 wt % solution.

### Sample preparation for interface studies

Samples for interface studies should be thin enough to shorten the analysis time in DSIMS measurement. Thus, thinner films of polyimides (~ 0.3 $\mu$m) were fabricated for this reason. A silicon wafer was diced into 1.27 × 1.27 cm dies and each silicon die was surface cleaned by using SC-1 cleaning before use. Thin films of polyimide BPDA-PPD and polyimide PMDA-ODA were formed by spin coating PI-2613 and

diluted PI-2808 solution, respectively, by using the following procedure: ramp to 1000 rpm in 1 s and hold at 1000 rpm for 1 s, ramp to 2000 rpm in 1 s and hold for 1 s, ramp to 3000 rpm in 1 s and then hold for 30 s, finally, ramp to 0 rpm in 1 s. This whole process could be simply expressed as 1000 rpm (1 s, 1 s), 2000 rpm (1 s, 1 s), and 3000 rpm (1 s, 30 s), and this expression will be used in the following sections. The specimens were then soft baked on a 110°C hot plate for 1 min and cured in a vacuum annealer under vacuum with continuous $N_2$ purge. The chamber pressure was kept at 300 mPa during the curing. Two different curing cycles were used to achieve either a fully cured or a partially cured PI base layer. The cured PI film was overcoated with a *d*-ATSP oligomer solution which was injected onto the substrate from a syringe, equipped with a Fluoropore® filter head. The following spin-coating parameters were used: 1000 rpm (1 s, 1 s), 2000 rpm (1 s, 1 s), 3000 rpm (1 s, 3 s). The coating was then soft baked by using IR radiation for 1 min at 170°C. The two layers were then cured at 240°C for 4 h in the vacuum annealer under house vacuum and $N_2$ purge. Last, the samples were annealed at 350°C for 4 h in vacuum to fully cure both polyimides and ATSP. This mimicked the temperature that bonded samples experienced during the ITR solid-state bonding process. The samples were then ready for the DSMIS study of the interface between the base polyimide layer and the top *d*-ATSP layer.

### Solid-state bonding of polyimide using ATSP

Four-micron-thick PI BPDA-PPD films were obtained by spin coating PI-2611® at 1400 rpm for 30 s followed by 4000 rpm for another 30 s on silicon substrate with chromium on the surface as the adhesion promoter. The films were then cured on a hot plate by ramping at 1°C/min to 350°C and then held at 350°C for 1 h. The ATSP oligomer solution was injected from a syringe, equipped with a Fluoropore® filter head to the substrate, and spin coated at 5000 rpm for 3 s. The coated substrates were cured under vacuum. The curing cycle involved (1) ramping from RT to 240°C at 2°C/min, (2) holding at 240°C for 4 h, (3) ramping to 280°C at 2°C/min, (4) holding at 280°C for 4 h, (5) ramping to 300°C at 2°C/min, (6) holding at 300°C for 4 h, and (7) cooling to RT at 2°C/min. The thickness of the cured film was measured at 0.3 $\mu$m with a Tencor $\alpha$-stage.

The cured 4-in. wafers were spin coated with photoresist AZ 5214EIR (PR) at 3000 rpm for 30 s and were soft baked on a 110°C hot plate for 30 s. The PR layer was used as a protective coating to prevent any scratching or embedding of silicon particles during the wafer-cleaving process. The wafers were cleaved into 1 × 1 cm squares, rinsed with acetone to strip PR, and baked at 110°C for 10 min. The cleaned specimens were inspected and those with defects at the edges of the silicon or in the film were eliminated (~ 50%). To prevent contamination of the samples outside the clean room, each set of specimens for bonding was pressed together by hand before taking out of the clean room. With the ATSP surface of both samples facing each other, specimens were bonded in a $N_2$ atmosphere at 320°C and 35 psi pressure for 4 h.

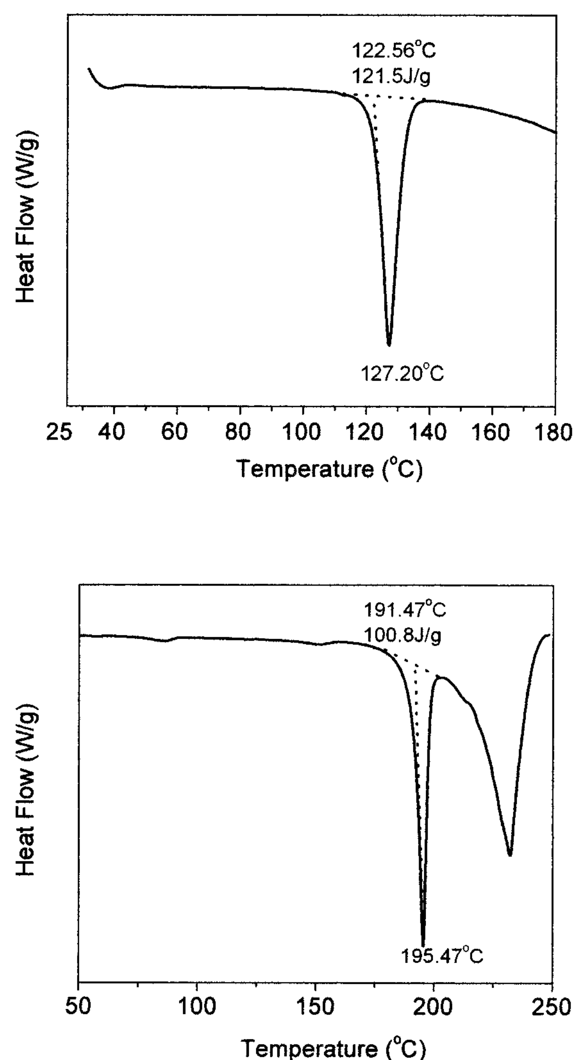


**Figure 3** DSC scan of *d*-HQDA (A) and *d*-ABA (B).

## RESULTS AND DISCUSSION

### Characterization of deuterated monomers and oligomers

As illustrated by DSC scans (Fig. 3), monomers with high purity were synthesized. *d*-HQDA has a single melting peak at 127.20°C (124.82°C for HQDA).[17] *d*-ABA has a melting peak at 195.47°C (196.55°C for ABA),[17] with the higher temperature endothermic peak indicating the sublimation of *d*-ABA at 230°C.

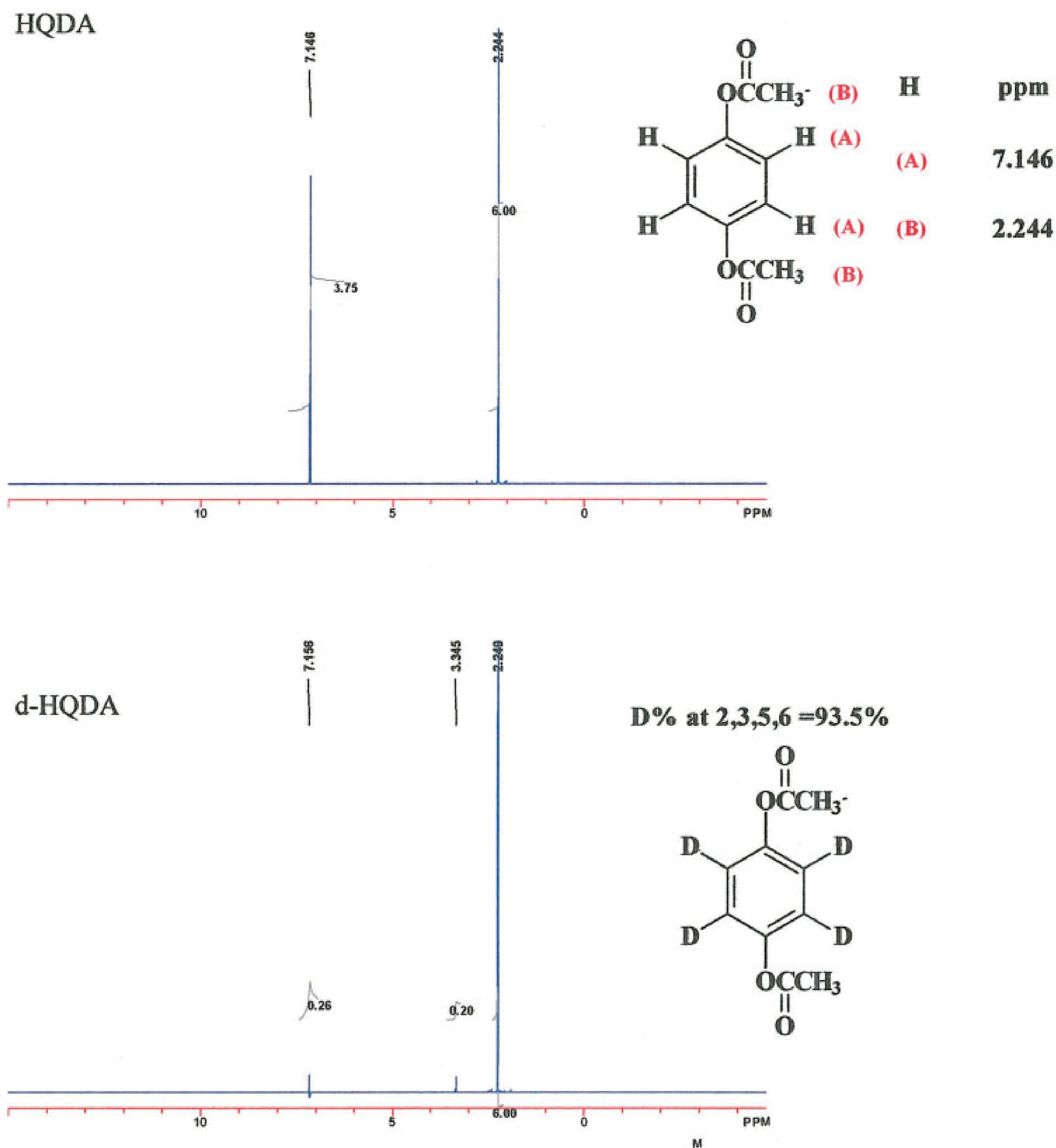


**Figure 4** ^{1}H-NMR spectra of HQDA and *d*-HQDA.

^{1}H-NMR spectra of monomers HQDA, *d*-HQDA, ABA, *d*-ABA have further demonstrated the high purity of the monomers (Figs. 4 and 5). In addition, by comparing the difference in integration values of the proton peaks from deuterated versus nondeuterated monomers, the percentage of deuterium replacement can be quantified. By using this procedure, it was found that the percentage of deuterium replacement is 93.5% at positions 2, 3, 5, and 6 on the HQDA benzene ring and is 81% at positions 3 and 5 on the ABA benzene ring. These results are consistent with the published literature.[16]

Purified oligomer C-1 and A-1 were characterized by DSC and showed a melting point around 160°C (Fig. 6). The oligomers could be readily dissolved in NMP without gel, and GPC characterization of $M_w$ could thus be performed; Figure 7 shows the GPC traces of C-1 and A-1, and the $M_w$ was calculated as between 6000 and 7000 for both C-1 and A-1 with a narrow polydispersity $< 1.2$. Based on the D% of *d*-HQDA, *d*-ABA, and the monomer ratio in the synthesis of C-1, A-1, the D% is calculated to be 42% in the deuterated ATSP oligomer C-1 and 58% in A-1. Because ATSP is cured from C-1 and A-1 with

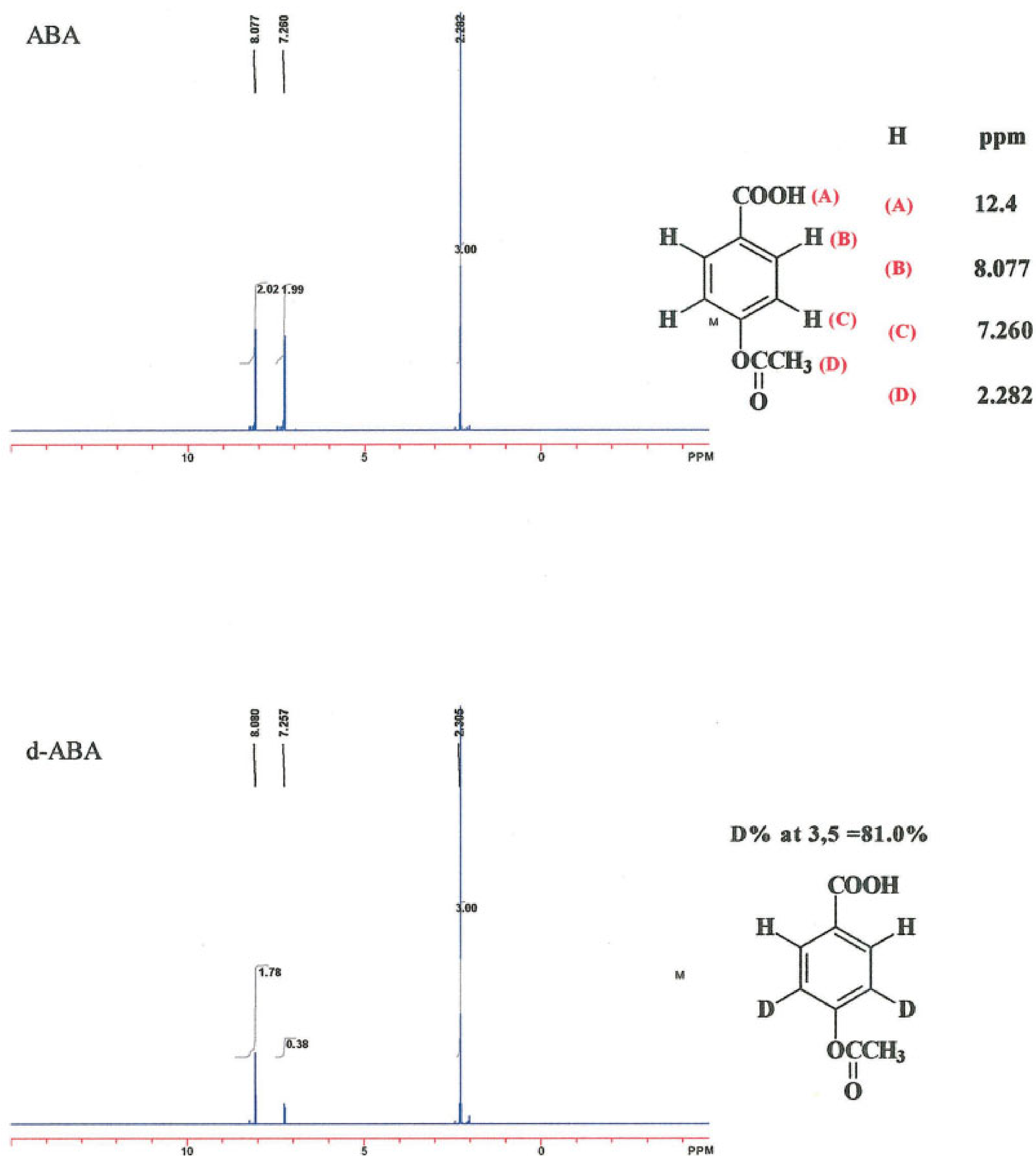


**Figure 5** $^1$H-NMR spectra of ABA and *d*-ABA.

1 : 1*M* ratio, the D% in cured ATSP is approximately 50%.

## Adhesion characteristics of ATSP (background)

In our previous publications,[12,18,19] it was reported that both liquid crystalline polyesters (LCP) and ATSP can form good adhesive bonds by heating at temperatures of 260–320°C and applying some pressure. In the case of the LCP, rather modest lap shear strength was observed of 10 MPa. Failure was invariably cohesive as might be predicted because of the relatively weak transverse properties of the LCP. To address this problem, we modified the LCP to have the ability to crosslink and thus produce a more isotropic adhesive bond. This led to the dis-

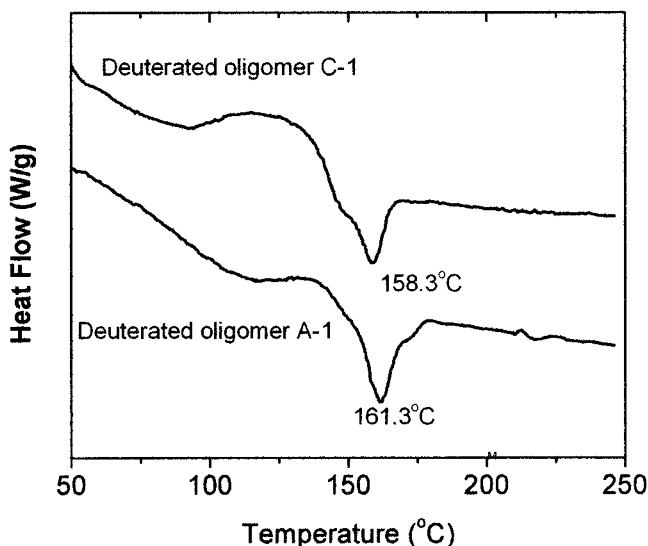


**Figure 6** DSC scans of deuterated oligomer C-1 and A-1.

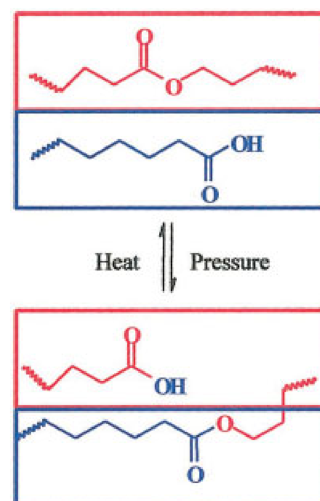


**Figure 8** Interchain transesterification reaction (ITR).

covery of ATSP, a new family of thermosets with a number of unique properties.[19]

Previously, ATSP was investigated as a high-temperature structural adhesive.[17] The substrate was first coated from the ATSP oligomer melt, obtained by heating the oligomer mixture to 200°C. The coating (100–125 $\mu$m) was then cured by heating to 240–320°C. Such coatings displayed the potential for further reaction at the interface via ITR in the solid state to achieve a strong adhesive bond with a similarly cured coating. The same principle of solid-state bonding was used in the following sections, with one distinctive difference, namely, the ATSP was used as an adhesive at submicrometer thickness.

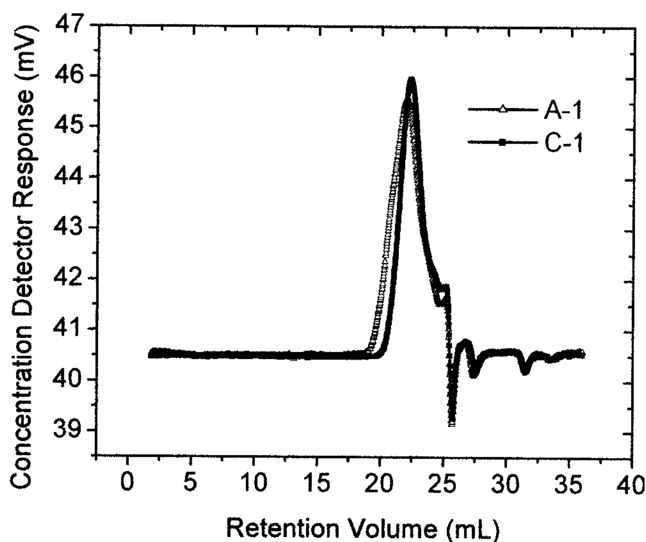


**Figure 7** GPC trace of optimized oligomer C-1 and A-1.

## Adhesion mechanisms

### ATSP–ATSP interface

The nature of the bonding between two ATSP-coated surfaces was shown to occur by ITR (Fig. 8).[18] As is shown in Figure 9, a seamless bond formed between two ATSP-coated silicon dies. The adhesion between the two dies was so good that stress was transferred through the adhesive and cleaved the bottom silicon die simply by cleaving the top silicon die. Further investigation has found that by using a partially cured ATSP layer instead of a fully cured one would further improve the extent of ITR.[20] The reasons are twofold, as follows: (1) the relatively lower $T_g$ and better chain mobility in the partially cured ATSP allow functional groups from the two layers of the cured ATSP to have intimate contact to promote ITR; (2) more active polar end groups, which have a faster ITR rate, would be

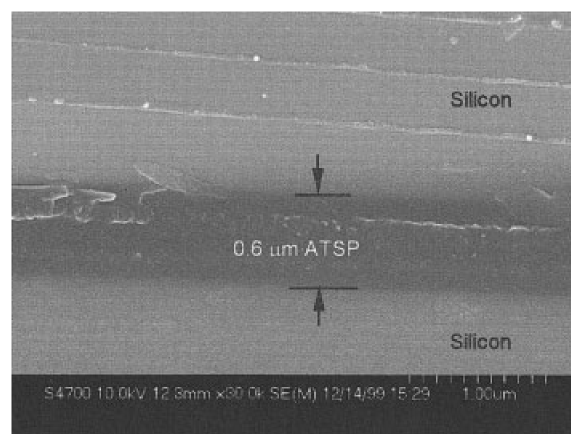


**Figure 9** $SiO_2$/ATSP/$SiO_2$ bond line cross section of silicon sample bonded using submicrometer ATSP.

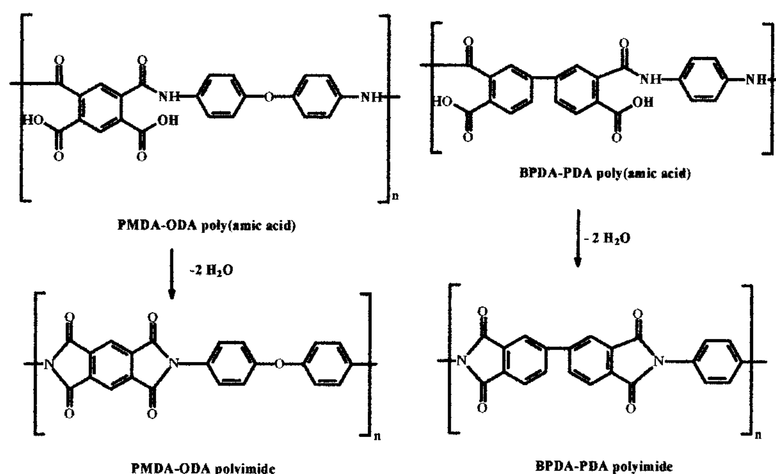


**Figure 10** Chemical structures of polyimides (a) PMDA-ODA and (b) BPDA-PPD.

available for further reaction in a partially cured ATSP than in a fully cured ATSP.

### ATSP–oxide interface

Silicon, silicon oxide, and aluminum have native silicon oxide, thermal silicon oxide, and aluminum oxide on their surfaces, respectively. The bonding of ATSP with these surfaces is likely due to the interaction of end groups (both —COOH and —OAc) with the polar groups on the surface of the substrates (e.g., metal oxide, silicon oxide) formed during the curing process, as well as dipolar interactions of the backbone aromatic ester group with the surface. The coating of oligomer solution and subsequent heating (curing process) allow oligomers to wet the substrate well, leading to intimate molecular contact with the surface, and provide enough time and temperature for the oligomer end groups to interact with the substrates. Jung and Czanderna studied the interaction of functional groups with metal oxide by using self-assembled monolayers that contain different functional groups and has ranked the different functional groups by their strength of interaction.[21] Among the functional groups studied, —COOH and —OAc were ranked in the top 1 category for most metal oxides. This may explain why ATSP has good adhesion with various substrates. Among the three surfaces, the native silicon oxide formed on silicon displays a high content of dangling —OH bonds as compared to the thermal oxide. This could provide some hydrogen bonding with the —COOH end groups, which can explain why Si-bonded samples, with native oxide on the surface, had the highest tensile bond strength among all the substrates. Among various attractive energies, chemical bonding would lead to the highest bonding energy, followed sequentially by hydrogen bonding, dipole–dipole attraction, dispersion force, and dipole-induced dipole attraction.[22] Further investigations on the interaction between ATSP and metal

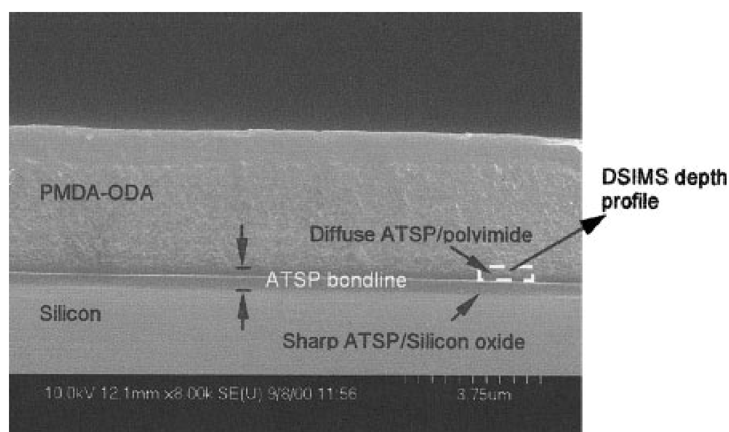


**Figure 11** Polyimide/ATSP/$SiO_2$ bond line cross section of a polyimide membrane transferred onto a silicon substrate using submicrometer ATSP.

oxide or silicon oxide would be of interest with the goal to replace the dipole–dipole interactions with chemical bonding because the latter has adhesion energies of 10–20 times higher.

## ATSP–polyimides interface

It is well known that much of the mechanical strength of a polymer originates from molecular entanglement. This accounts not only for the cohesive strength within the polymer, but also for the adhesive strength at the interface. In the case of polyimide, its poor self-adhesion originates from its semicrystalline structure, which limits the diffusion of the overcoated PAA top-layer chains into the bottom layer during the curing as well as the minimal ability for entanglement of the polyimide chains due to their extended chain conformation. Because ATSP oligomers have smaller $M_w$ (7000 versus 20,000–50,000) than PAA, and the crosslinking of ATSP oligomers is much slower than the imidization of polyamic acid, ATSP oligomers should have a better chance to diffuse further into a cured PI during the crosslinking of ATSP. It was also suspected that PI's packing density would affect the degree of ATSP oligomer's diffusion. Two representative polyimides PMDA-ODA and BPDA-PPD were used in this study. Their chemical structures are illustrated in Figure 10. Due to its flexible —O— linkage, PMDA-ODA has less rigid backbone compared with BPDA-PPD. It was found in the bonding experiments that ATSP provides relatively stronger adhesion with cured PI PMDA-ODA.[14]

The interface between PI and ATSP is shown in Figure 11. The example shown here is of a 4-$\mu$m PI PMDA-ODA transferred to a native oxide surface via solid-state bonding by ITR.[20] The interface between ATSP and PMDA-ODA was rather diffuse if compared with the interface of ATSP and the native oxide. Although SEM could give a rough image of the interface, it could not give a quantitative value of the interface width, which is essential in determining the adhesion strength at the interface of polyimides and ATSP. Hence, DSIMS was used to quantify the interface width. Before using DSIMS, the surfaces of the cured PI were inspected by using AFM and shown to be very smooth with a mean roughness less than 3 Å. Thus, if interface width is measured to be larger than the roughness, it would be due to the diffusion and not the natural topography of the PI surface.

DSIMS uses a beam of energetic (0.5–2.0 keV) primary ions to sputter the sample surface, producing ionized secondary particles that are detected by using a mass spectrometer (Figure 12).[23] Cs+ was chosen as the primary ion for obtaining electronegative species (C-, H1-, H2-, O-, etc.) and for better resolution. Depth profiles are obtained if one or more masses are monitored sequentially by switching rapidly among masses. Detailed information about DSIMS exists in the literature.[23] In the current experiments, secondary ions H1-, H2-, C-, O-, CN-, Si-, and Au- were detected. Among those secondary ions, H2- and CN- are representative ions of *d*-ATSP and polyimides, respectively. C- was used as an index of a constant sputtering rate and as an internal standard if comparing the H2-

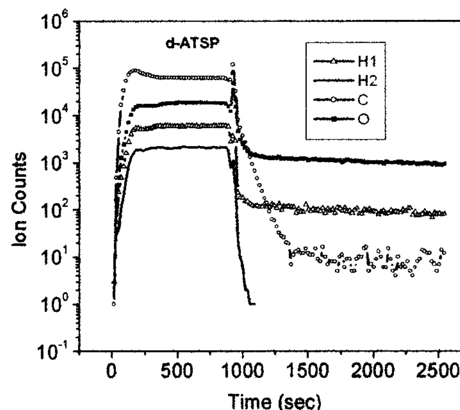


**Figure 13** Depth profile of *d*-ATSP.

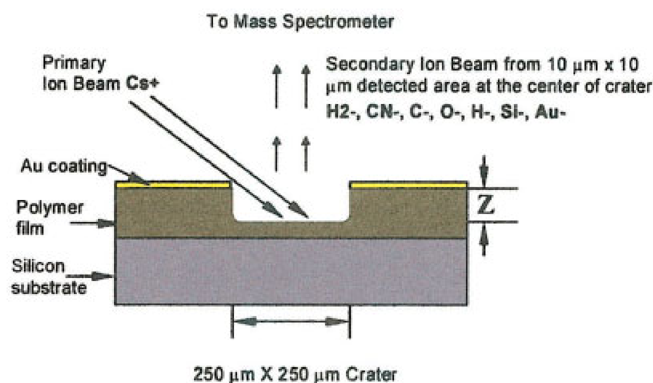


**Figure 12** Principle of depth profiling using dynamic secondary ion mass spectrometry.

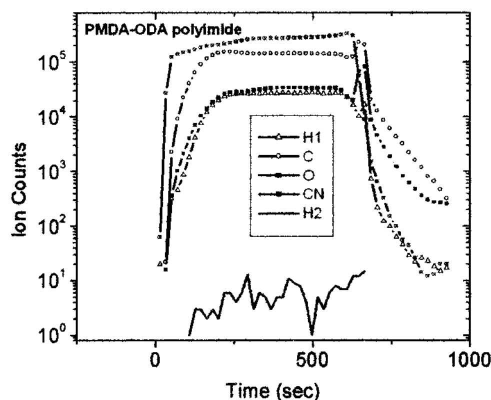


**Figure 14** Depth profile of PMDA-ODA polyimide.

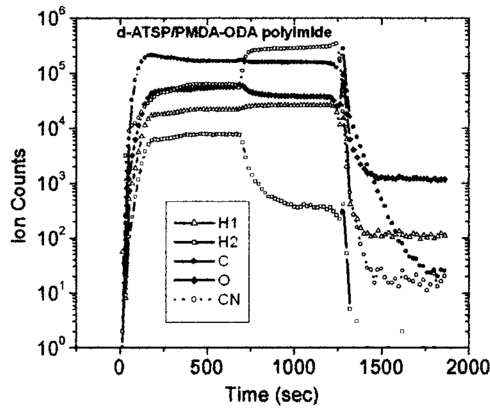


**Figure 15** Depth profile of a bilayer structure with *d*-ATSP coated on a fully cured PMDA-ODA polyimide layer.

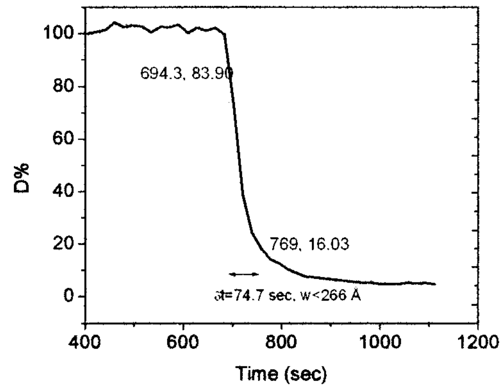


**Figure 17** Interface width of a bilayer structure with *d*-ATSP coated on a fully cured PMDA-ODA polyimide base layer.

concentration among different samples is needed. The appearance of Si- was used as an indication that the sputtering had reached the silicon substrate and the experiment could be stopped. A $10 \times 10$ $\mu$m detected region was chosen from the center of a $250 \times 250$ $\mu$m crater to eliminate the crater side-wall effect and thus ensure high resolution.[23]

The depth profiles of thin films of *d*-ATSP, PMDA-ODA polyimide, and double layers of *d*-ATSP coated on PMDA-ODA polyimide are shown in Figures 13, 14, and 15, respectively. The thickness of the films was measured by using a profilometer. The sputtering time was then converted into the depth based on film thickness. It could be seen from the spectra that *d*-ATSP is very rich in deuterium, allowing for quantification of the diffusion study of *d*-ATSP oligomers.

As shown in Figure 16, at an interface, the derivative of the depth profile is an error function and the $\pm\sigma$ points correspond to 84 and 16% of maximum intensity. The interface width was determined as $2\sigma$. An expression $<$ should be used to describe the interface width. Because the machine error also contributes to the interface width, the value of a true interface width is always smaller than the calculated value using error function. The interface width between a fully cured PMDA-ODA base layer with ATSP and between a fully cured BPDA-PPD base layer with ATSP were determined in this manner, as shown in Figures 17 and 18, respectively. The former was found to be twice the latter, indicating a more diffuse interface was observed between PMDA-ODA and ATSP. It is understandable because PMDA-ODA has an —O— linkage in the structure, which provides a certain degree of flexibility to the PMDA-ODA chain, compared to the rodlike BPDA-PPD. Therefore, it is easier for the ATSP oligomers to diffuse into the PMDA-ODA. The DSIMS measurements conclusively answered the questions concerning the better adhesion seen in PMDA-ODA when bonded using ATSP.

Although PMDA-ODA shows less dense packing than BPDA-PPD, a lower density packing should be seen in the polyamic acid precursors. To improve polyimides' self-adhesion, partial curing of the base

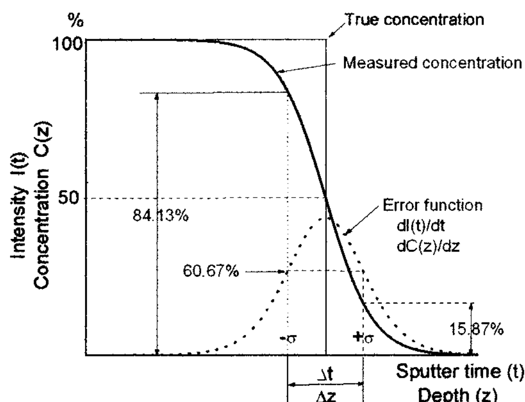


**Figure 16** Depth profile parameters for the analysis of an interface described in terms of sputter time or depth.

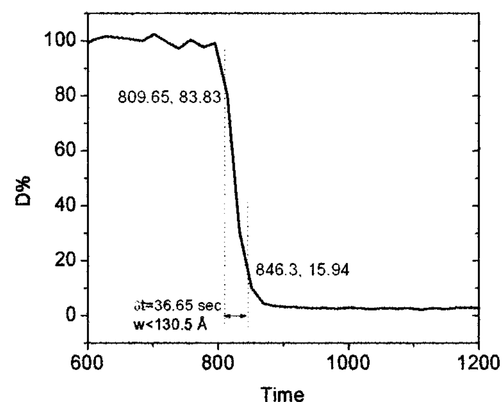


**Figure 18** Interface width of a bilayer structure with *d*-ATSP coated on a fully cured BPDA-PPD polyimide base layer.

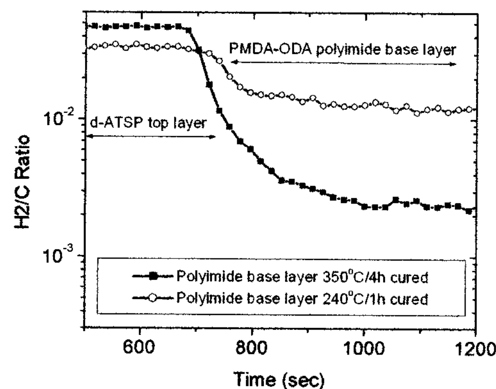


**Figure 19** Comparison of the interface of ATSP/fully cured PMDA-ODA polyimide with the interface of ATSP/partially cured PMDA-ODA polyimide.

polyimide[24] or a KOH/HCl wet chemistry surface treatment[25] were both used to provide some amount of the more flexible polyamic acids at the surface. In this study, the interface between ATSP with either a partially cured PMDA-ODA or a partially cured BPDA-PPD was investigated by using DSIMS. Both polyimides were partially cured at 240°C for 1 h (imidization degree is 60%).[4] As shown in Figures 19 and 20, in both cases, the interfaces involved with partially cured polyimides are much more diffuse than their fully cured versions, and considerable concentration of *d*-ATSP has diffused into the partially cured polyimides base layer. Table I lists the width of the four different interfaces, which indicates the use of a partially cured BPDA-PPD could improve BPDA-PPD's adhesion with ATSP.

## CONCLUSION

ATSP can be used as a submicrometer thin-film adhesive to bond various substrates in the solid state via ITR, providing a unique pathway to integrate prefabricated components into a functional device in microelectronic fabrication. It is believed that the adhesion mechanism between ATSP and silicon oxide or metal oxide is primarily due to the dipole–dipole attraction, while the adhesion between ATSP and native silicon oxide has a contribution from hydrogen bonding. The adhesion strength at the interface between ATSP and polyimides is strongly related to the diffusion of ATSP into the polyimide base layer. DSIMS was used to study the interface width between ATSP and polyimides and it was found that the interface between ATSP and polyimide PMDA-ODA is wider than the interface between ATSP and polyimide BPDA-PPD, due to the less rigid chain in the polyimide PMDA-ODA. By partially curing both polyimides, the interface width was greatly increased, which could lead to an improved adhesion at the interface between PI BPDA-PPD and ATSP.

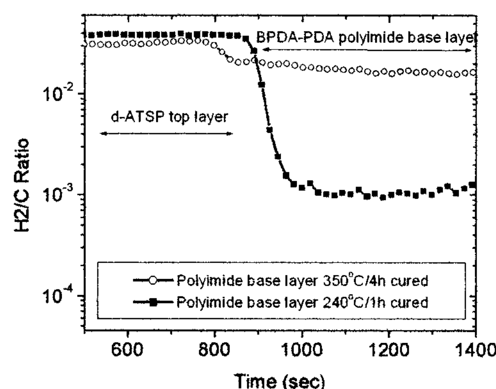


**Figure 20** Comparison of the interface of ATSP/fully cured BPDA-PPD polyimide with the interface of ATSP/partially cured BPDA-PPD polyimide.

**TABLE I**
**Interface Width of Polyimide/ATSP**

| | PMDA-ODA fully cured | PMDA-ODA partially cured | BPDA-PPD fully cured | BPDA-PPD partially cured |
|---|---|---|---|---|
| W (Å) | <266 | <466 | <130.5 | <602 |

This work was supported by DARPA DSO (Contract DABT63-97-C-0069). The thin-film analysis was carried out in the Center for Microanalysis of Materials, University of Illinois, which is partially supported by the U.S. Department of Energy under Grant DEFG02-91-ER45439. The authors thank the following staff at the Center for Microanalysis of Materials for assistance in various analytical metrologies: Judy Baker for the DSIMS, and Nancy Finnegan and Jim Mabon for the AFM.

## References

1. Brown, H. R.; Yang, A. C. M.; Russell, T. P.; Volksen, W.; Kramer, E. J. Polymer 1988, 29, 1807.
2. Mittal, K. L. Polyimides: Synthesis, Characterization, and Applications 1–2; Plenum Press: New York, 1984.
3. Nese, M.; Hannerborg, A. Sens Actuat A 1993, 37–38, 61.
4. Stoffel, N. C.; Dai, C.-A.; Kramer, E. J.; Russell, T. P.; Deline, V.; Volksen, W.; Wu, W.; Satija, S. Macromolecules 1996, 29, 6880.
5. Stoffel, N. C.; Kramer, E. J.; Volksen, W.; Russell, T. P. Polymer 1993, 34, 4524.
6. Jones, R. A. L.; Norton, L. J.; Kramer, E. J.; Bates, F. S.; Wiltzius, P. Phys Rev Lett 1991, 66 (10), 1326.
7. Furman, B. K.; Childs, K. D.; Clearfield, H.; Davis, R.; Purushothaman, S. J Vacuum Sci Technol A 1992, 4, 2913.
8. Stoffel, N. C.; Hsieh, M.; Kramer, E. J.; Volksen, W. IEEE Trans Compon Packag Manuf Technol B 1996, 19, 417.
9. Maas, D.; Bustgens, B.; Fahrenberg, J.; Keller, W.; Seidel, D. 4th International Conference on New Actuators; Bremen, Germany, 1994; pp 75–78.
10. Mass, D.; Bustgens, K.; Fahrenberg, J.; Keller, W.; Ruther, P.; Schomburg, W. K.; Seidel, D. Proceedings of the 1996 IEEE Micro Electro Mechanical Systems Workshop, San Diego, CA, 1996; pp 331–336.

11. Lee, K.-W.; Viehbeck, A.; Walker, G. F.; Cohen, S.; Zucco, P.; Chen, R.; Ree, M. J Adhes Sci Technol 1996, 10, 807.
12. Frich, D.; Economy, J.; Goranov, K. Polym Eng Sci 1997, 37, 541.
13. Xu, K.; Economy, J.; Shannon, M. A. Int J Microcircuits Electron Packag 2000, 23, 78.
14. Selby, J. C.; Shannon, M. A.; Xu, K.; Economy, J. Micromech Microeng 2001, 11, 672.
15. Shannon, M.; Philpott, M.; Miller, N.; Bullard, C.; Beebe, D.; Jacobi, A.; Hrnjak, P.; Saif, T.; Aluru, N.; Sehitoglu, H. Rocket, A.; Economy, J. Proc ASME, Adv Energy Sys Div 1997, 75.
16. Niessner, N.; Muehlebach, A.; Lyerla, J. R.; Facey, G. A.; Fyfe, C. A. Makromol Chem 1993, 194, 649.
17. Xu, K. Ph.D. Thesis, University of Illinois at Urbana-Champaign, 2002.
18. Frich, D.; Hall, A.; Economy, J. Macromol Chem Phys 1998, 199, 913.
19. Frich, D.; Goranov, K.; Schneggenburger, L.; Economy, J. Macromolecules 1996, 29, 7734.
20. Selby, J. C. Master Thesis, University of Illinois at Urbana-Champaign, 2001.
21. Jung, D. R.; Czanderna, A. W. Crit Rev Solid State Mater Sci 1994, 19, 1.
22. Wu, S. Polymer Interface and Adhesion, 1st ed.; Marcel Dekker: New York, 1982.
23. Wilson, R. G.; Stevie, F. A.; Magee, C. W., Eds. Secondary Ion Mass Spectrometry: A Practical Handbook for Depth Profiling and Bulk Impurity Analysis; Wiley: New York, 1989.
24. Brown, H. R.; Yang, A. C. M. J Adhes Sci Technol 1992, 6, 333.
25. Lee, K.-W. J Adhes Sci Technol 1994, 8, 1077.